RSC Advances

ROYAL SOCIETY
OF CHEMISTRY

www.rsc.org/advances

Expert Construction of Heterostructured InCrO$_4$−TiO$_2$ and Its Dual desk Application of Greater UV- Photocatalytic and Antibacterial Activity

J. Kamalakkannan, V.L.Chandraboss, S. Prabha and S. Senthilvelan*

Department of Chemistry, Annamalai University, Annamalainagar 608 002.

E-mail: dr_senthilvel@yahoo.co.in

Graphical abstract

Expert recylable heterostructured InCrO$_4$−TiO$_2$ prepared by a simple co-precipitation method, mechanisam of holes and electrons exhibits high UV-Photocatalytic activity and antibacterial activity.
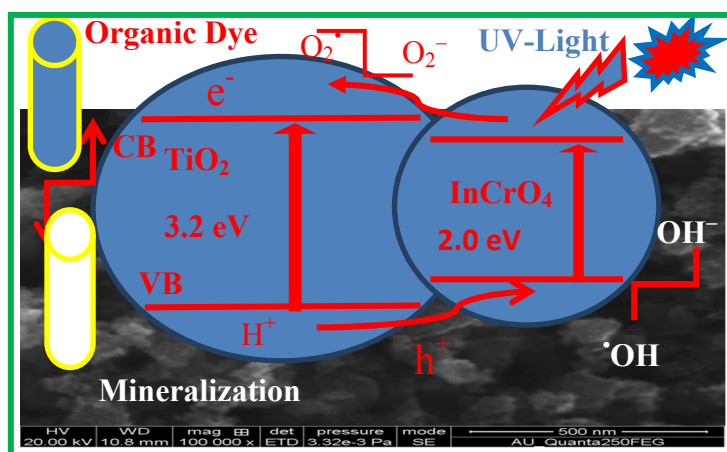
Expert Construction of Heterostructured $InCrO_4$−TiO_2 and Its Dual desk Application of Greater UV- Photocatalytic and Antibacterial Activity

J. Kamalakkannan, V.L. Chandraboss, S. Prabha and S. Senthilvelan*

Department of Chemistry, Annamalai University, Annamalainagar 608 002.

E-mail: dr_senthilvel@yahoo.co.in

ABSTRACT

Development of coupled semiconductor oxides makes a significant advancement in the photocatalytic functional materials. In this article, we report the preparation of nano-spherical $InCrO_4$-loaded TiO_2 photocatalyst by a simple Co-precipitation method. $InCrO_4$-TiO_2 (ICT) nano material was characterized by XRD, SEM with EDX, FT-IR, FT-RAMAN and PL analysis. The photocatalytic activity of $InCrO_4$−TiO_2 was much better activity than that of TiO_2 and TiO_2-P25 under UV-light irradiation. $InCrO_4$−TiO_2, TiO_2 and TiO_2-P25 is more advantageous than the degradation of methyl green (MEG), malachite green (MAG) and methylene blue (MB) because it has maximum efficiency at neutral pH=7 under UV-light irradiation. Among all these dyes the photodegradation of MEG was faster compared to other dyes. The photodegriedation due to MEG was studied the mechanism of photocatalytic effect of $InCrO_4$ loaded TiO_2 nanomaterial, hydroxyl radical analysis - Fluorescence technique with coumarin has been discussed Photocatalytic reaction used material and kinetics first order reaction, analyzed to be pseudo-first order by high quantum yield found to be calculated. Further antibacterial activity of the TiO_2 and $InCrO_4$-TiO_2 was investigated against gram negative *Vibrio cholera* and gram positive *Bacillus subtilis* bacterial strains.

Keywords: $InCrO_4$-TiO_2, Nanomaterial, Co-precipitation, Photocatalysis, Antibacterial activity.

1. Introduction

The dye from industrial effluents often poses a major environmental problem. Various dyes have been used in textile, dyeing, paper, pulp, plastic, leather, cosmetics and food industries,[1] Colour dye stuff discharge from these industries possess certain hazards and environmental problems.[2] Photocatalysis is one of the new techniques for removal of dyes from wastewater.[3-6] In this regard, some reported metal oxides nanocomposite revealed excellent photocatalytic performances.[7-9] Nowadays more than 9000 different types of dyes have been incorporated in the colour index.[10] MEG is one of the most common dying materials for wood, silk and cotton.[11] Titanium dioxide used in the paper, paint and plastics industries due to its excellent optical properties. The use of TiO_2 as a semiconductor photocatalyst is an efficient method for elimination of environmental pollutants, the degradation of organic contaminants from water has been reported and researched under various contexts.[12] In addition, titania doped with metal molybdates[13] were reported to have improved photocatalytic properties with enhanced absorption of visible/ ultraviolet light TiO_2 presents a relatively high electron‑hole recombination rate due to its wide band gap energy (ca. 3.0 eV for rutile and 3.2 eV for anatase), and as a result retards its photoactivity of a multicomponent system also depends on the synthetic procedure and their compositions. In recent years, binary metal oxides such as TiO_2/Fe_2O_3, TiO_2/WO_3, TiO_2/MoO_3, TiO_2/SiO_2 and TiO_2/ZrO_2 have been widely studied for their unique chemical, physical and photocatalytic properties.[14-18] Jiang Yin et al reported that $MCrO_4$ (Ba, Sr) has photocatalytic properties[19] but interestingly no one have studied on the photocatalytic properties of $SrCrO_4/TiO_2$ mixed oxides. The results revealed that the photocatalytic activity of $InCrO_4-TiO_2$ was much higher than that of TiO_2 and TiO_2-P25 under UV-light irradiation.

InCrO$_4$−TiO$_2$, undoped TiO$_2$ and TiO$_2$-P25 is more advantageous than the degradation of MEG, MAG, and MB because it has maximum efficiency at neutral pH=7. Photodegradation and decolorization of Methyle green (MEG) was fast photocatalytic activity. The photodegried due of MEG was shedied, different calcinations as the function of temperature of InCrO$_4$-TiO$_2$ (200, 300, and 450^{0}C), different concentrations of MEG (1×10^{-4} and 2×10^{-4}) dye and different catalyst loadings. Among the catalyst only InCrO$_4$-TiO$_2$ showed. Further antibacterial activity in recent times, the World Health Organization reports that at least 75 - 95% of the world populations of developing countries were mainly rely on traditional medicines and major fraction of traditional therapies absorbs the use of plant extract products or their active constituents[20]. Traditional medicine treatment is a frequent practice in developed and developing countries at the primary healthcare level.[21] Due to amplified and unsystematic use of antibiotics for treatment of humans and animals develops the antibiotic resistance and multidrug resistance microorganisms which has increased a great deal in developing countries.[22] The requirement of more and more drugs from plant sources is constantly increasing which necessitates screening medicinal plants with promising biological activity.[23] Many metabolites isolated from marine algae have been shown to possess bioactive efforts,[24] nd in- vitro antiproliferative activity in cancer cell lines.[25] In the present investigation the antibacterial activity of different solvent extracts were investigated against a range of gram positive and gram negative bacterial strain of the TiO$_2$ and InCrO$_4$-TiO$_2$ was investigated antibacterial activity and gram positive (a) *Bacillus subtilis* and against gram negative (b) *Vibrio cholera* antibacterial activity of bacterial strains.

2. Experimental

2.1. Synthesis of InCrO$_4$-TiO$_2$ nanomaterial

Nanomaterial mixed oxide photocatalysts InCrO$_4$-loaded TiO$_2$ (ICT) were prepared by co-precipitation method. The total synthesis was carried out in two steps. A typical synthesis of InCrO$_4$ was conducted in the following way, InCl$_3$ and ((NH$_4$)$_2$Cr$_2$O$_7$.2H$_2$O) were first dissolved with distilled water respectively, the as prepared InCl$_3$ solution was put in a beaker, and then slowly added ((NH$_4$)$_2$Cr$_2$O$_7$.2H$_2$O reached 1:1 continual magnetic stirring for 2 h was required to keep the reactant mixed uniformly, the pH value solution being adjusted to about 9 with ammonia solution added. After that, they obtained solution was placed in a sonication for 20 mins respectively precipitat was formed. Obtained precipitate was filtered and washed with distilled water for three to five times to remove the remaining Cl$^-$ and NH$_4^-$. Finaly sample was dried at 100 ^{0}C for 1 h. In the second step the The resulting solution was added dropwise into tetra isopropyl orthotitanate solution with anhydrous ethanol as solvent at room temperature under vigorous stirring 4 h until precipitate formed was placed in sonication 20 mins. The obtained precipitate was was filtered and washed with distilled water and ethanol until alkali phases were removed from precipitation. Then the precipitate was collected and dried in oven at 100 ^{0}C for 12 h. The resulting powder was finally calcined at 200, 300 and 450 ^{0}C for 3 h. The heat treatment of the sample at a temperature higher than 300 °C had poor photocatalytic activity shown in Sheme.1.

2.2. Materials

Tetra isopropyl orthotitanate (C$_{12}$H$_{28}$O$_4$Ti), ammonium dichromate dihydrad ((NH$_4$)$_2$Cr$_2$O$_7$.2H$_2$O-analytical reagent), Indium chloride (InCl$_3$), NH$_3$ solution, nitric acid (HNO$_3$-65%), malachite green (C$_{23}$H$_{25}$ClN$_2$), methyl green (C$_{26}$H$_{33}$N$_3$Cl$_2$) and methylene blue

$(C_{18}H_{18}N_3SCl_3H_2O)$, were used as such. A gift sample of TiO_2-P25 (80% anatase), ethanol, tBuOH, coumarin (1 mM of 4-hydroxycoumarin) and double distilled water were the guaranteed reagents of Sigma Aldrich and used as such. Chemical structure of methyl green is shown in Fig. 1. The aqueous solutions were prepared by using double distilled water. All glassware's were cleaned with chromic acid followed by thoroughly washing with distilled water.

2.3. Photocatalysis

The reaction out by using multilam photoreactor with 365 nm UV lamps. The reaction was maintained at ambient temperature (303 K). In a typical experiment aqueous suspensions of dye (40 mL, 1×10^{-4} M) and 0.150 g of the photocatalyst were loaded in reaction tubes. Prior to irradiation, the suspension was magnetically stirred in the dark to ensure the establishment of an adsorption/desorption equilibrium. The suspension was kept under constant air-equilibrated condition. At the time intervals of given irradiation time. The suspension was measured spectrophotometrically at 630 nm (MEG), 620 nm (MAG) and 665 nm (MB) within the Beer–Lambert law limit.

2.4. Analysis of hydroxyl radical ($^•$OH)

Detection of hole and hydroxyl radical species, the examination experiment process of hole and hydroxyl radical species is similar to the photocatalytic activity experiment. A different quantity of scavengers only inhibited when the hydroxyl radical scavenger tBuOH was added was that holes and hydroxyl radicals are the main active species involved in the decomposition of the adsorbed organic pollutants. Introduced into the MEG solution prior to addition of the catalyst. In addition of UV-light irradiation for every 0, 30 and 60 mints, this result suggests that the fluorescence arises[53] from the chemical reactions between coumarin solution and $^•$OH formed on the illuminated $InCrO_4-TiO_2$ by UV irradiation for 60 min.

2.5. Determination of antibacterial activity by disc diffusion method

Nutrient agar plates were prepared under sterile conditions and incubated overnight to identify contamination. About 0.2 mL of working stock culture was shifted into separate nutrient agar plates and spread thoroughly using a glass spreader. Whatmann No.1 discs (6 mm in diameter) were impregnated in the testing compounds dissolved in DMSO (200 mg/mL) for about half an hour. Commercially available drug disc, Ciprofloxacin (10 mg/disc) was used as positive reference standard. All the compounds were tested at dose levels of 1000 µg and DMSO used as a control. The solutions of each test compound, control and reference standard were added separately in the cups and the plates were kept undisturbed for at least 2 hours in a refrigerator to allow diffusion of the solution properly into nutrient agar medium. Petri dishes were subsequently incubated at 37±1 0C for 24 hours. After incubation, the diameter of zone of inhibition surrounding each of the cups was measured with the help of an antibiotic zone reader.[26]

2.6. Characterization

X-ray diffraction (XRD) spectra was recorded on the X'PERT PRO model X-ray diffractometer from Pan Analytical instruments operated at a voltage of 40 kV and a current of 30 mA with Cu Kα radiation.

Scanning electron microscopy (SEM) with elementary dispersive X-ray (EDX) analysis was carried out on a FEI Quanta FEG 200 instrument with EDX analyzer facility at 25 °C. The sample was prepared by placing a small quantity of prepared material on a carbon coated copper grid and allowing the solvent to evaporate.

Fourier transform-infrared spectrum (FT-IR) was recorded using SHIMADZU FT-IR spectrometer in KBr pellet.

FT-RAMAN spectra were recorded with an integral microscope Raman system RFS27 spectrometer equipped with 1024 – 256 pixels liquefied nitrogen-cooled germanium detector. The 1064 nm line of the Nd:YAG laser (red laser) was used to excite. To avoid intensive heating of the sample, the laser power at the sample was not higher than 15 mW. Each spectrum was recorded with an acquisition time of 18 s.

Photoluminescence (PL) spectra at room temperature were recorded using a Perkin-Elmer LS 55 fluorescence spectrometer. Nanoparticles were dispersed in carbon tetra chloride and excited using light of wavelength 300 nm. Ultraviolet and visible (UV-vis) absorbance spectra were measured over a range of 800-200 nm with a Shimadzu UV-1650PC recording spectrometer using a quartz cell with 10 mm of optical path length.

Fulorescence technique with coumarin (1 mM of 4-hydroxycoumarin) were measured on a Hitachi F-7000 fluorescence spectrophotometer.

3. RESULTS AND DISCUSSION

3.1. XRD analysis

The obtained XRD of the TiO_2 and $InCrO_4 - TiO_2$ nanomaterial, are shown in Fig. 2a and 2b. The TiO_2 peaks at 15.62, 25.22, 29.02, 37.54, 48.12, 54.27, and 63.37, are the diffractions of the TiO_2 (100), (101), (101), (004), (200), (211) and (204) crystal planes diffractions peaks of anatase phase TiO_2 (JCPDS No. 21-1272). $InCrO_4 - TiO_2$ peaks at 21.02, 25.27, 27.37, 31.07, 38.05, 48.12, 54.82, and 62.02 are the diffractions of the ICT (100), TiO_2 (101), ICT (200), ICT (112), ICT (202), TiO_2 (200), TiO_2 (211) and ICT (400) crystal planes respectively diffractions peaks of $InCrO_4$ (JCPDS No. 01-088-0110). The two samples of TiO_2 and $InCrO_4 - TiO_2$

exhibited a diffraction pattern of FCC crystal structure. The average crystalline size (L) of the TiO$_2$ and InCrO$_4$ –TiO$_2$ particles can be calculated from the Debye–Scherrer formula, L=0.89λ/βCOSθ where L is the crystalline size (in nm), l is the wavelength (in nm), b is the full width at half maximum intensity (FWHM-in radian), and u is the Bragg diffraction angle (8). The average crystalline size of TiO$_2$ and InCrO$_4$ –TiO$_2$ product synthesized was figured out to be about 78.9 nm.

3.2. SEM with EDX analysis

SEM micrograph of the calcined (450^{0}C) pure TiO$_2$ and InCrO$_4$-TiO$_2$ nanomaterials is shown in (Fig. 3a and Fig.4a and 4b) this images show used to examine the Morphology and topography of prepared materials. In this article, we report the image of the prepared nano spherical-shaped InCrO$_4$-loadeed TiO$_2$ photocatalyst, revealed that individual particles were particles of various shapes with an average size of 80 nm. The shape of the InCrO$_4$-TiO$_2$ material revealed by SEM is in agreement with the results observed by XRD. Since the technique employed for the loaded TiO$_2$ has a strong influence on the morphology of the final material, further EDX analysis confirms only Titanium and Oxygen present in undoped TiO$_2$, Where as Indium, Chromate, Titanium and oxygen are present in InCrO$_4$-TiO$_2$. EDX analysis of the nanomaterial sample confirms (Fig. 3b and 4c). Than image profile and plot profile of the selected area in (Fig. 3C, 3d and Fig.4d, 4e) of the TiO$_2$ and InCrO4-TiO$_2$ nanomaterial

3.3. FT-IR analysis

In order to investigate the surface characteristics of TiO$_2$ and InCrO$_4$- TiO$_2$ before and after treatment with methyl green dye, The IR spectrum of the Fig.5a. TiO$_2$ shows the absorption peaks at 3750, 3370, 1640, 1550, 1400, 1250, 1140, 1180, 967, 852, 787, 683 and 482 cm^{-1} respectively. The band at 3750 is due to NH$_2$. While 3370 shows OH carboxylic acid, 2341 are due to C≡C ring, 1640 cm^{-1} is due to S-H$_2$O, 1550 cm^{-1} is due to O-H, 1400 is due to C-H

bonds[27] 1205.55 shows C-N amine group. 852cm-1 is due to C-O[28] bond the main absorption peaks at 482, 671 and 787 cm^{-1} was assigned[29-32] to the Ti-O and Ti-O-Ti bonds. Fig.5b The FTIR spectrum of InCrO$_4$- TiO$_2$ before treatment on Methyl green shows the peak positions are at 3750, 3368, 2922, 2852, 2405, 2328, 2357, 1745, 1629, 1398 and 478 cm.$^{-1}$ The band at 3750-3368 is due to NH$_2$. While 2922, shows C-H band aliphatic , 2357 is shows C=N nitrate group, 1745 is shows C=O, 1629 is shows S-H$_2$O bands,[33-35] 1398 is due to O-H group[36] and 478cm^{-1} is due to Ti-In-Cr-O-Ti bonds. Fig.5c The FTIR spectrum of InCrO$_4$- TiO$_2$ affter treatment on Methyl green shows the peak positions are at 3700, 3250, 2920, 1750, 1620, 1400 1300 and 473 cm.$^{-1}$ The band at 3700-3250 shows NH$_2$ group aliphatic and aromatic group, 2920 shows C-H aliphatic group, 1750 is shows C=O bands, 1629 is shows S-H$_2$O bands, 1300 is due to O-H group, C=O that OR aromatic, C-N amine group and 473 cm^{-1} Ti-In-Cr-O-Ti bonds. The degradation of dye was measured by TOC determination. Degree of mineralization was determined using a total organic carbon (TOC) analyzer. The degradation of dye was measured determination. Degree of mineralization was determined using a total organic dye analyzer. Samples consisting of 40ml were taken at different time intervals of 40 mL were taken methyl green was prepared with the catalyst of 0.15 mg/L different time intervals used. The results show that mineralization is a slow process, requiring longer time for a complete mineralization. After 60 minute total degradation and decolorization is reached catalytically, whereas only 92.8% of TOC is removed by mineralization was observed. Total organic carbon reduction of MEG with respect to time over the InCrO$_4$-TiO$_2$ nanomaterial.

3.4. FT-Raman analysis

Anatase TiO_2 is body centred tetragonal (space group D4h, I41/amd, with an elongated cell having a = 0.3783 and c = 0.951nm) and contains two primitive unit cells, each of which contains two formula units of TiO_2[37]. According to the factor group analysis, six modes of anatase TiO_2, A1g + 2B1g + 3Eg are Raman active and three modes, A2u + 2Eu, are infrared active One vibration, B2u, will be inactive in both infrared and Raman spectra. All of these modes account for the 15 normal modes of vibration. Thus group theory predicts six Raman active modes for the tetragonal anatase phase: three Eg modes centred on 145, 197, and 639 cm^{-1}; two B1g modes at 399 and 519 cm^{-1}; and one A1g mode at 513 cm^{-1} respectively[38]. Fig.6. presents the spectrum $InCrO_4$-TiO_2 consists of three peaks located at about 1084, 897, 871, 834, 785, 621, 555, 446, 415, 397, 287, 235 and 145cm^{-1} predominantly for the main peak around 145 from 621.68 to 397.97 cm^{-1}. It has been known that the shift of the peak position and change of thewith related to changes of surface oxygen deficiency. The blue shift and decrease in peak broading demonstrated that the content of Oxygen deficiency increased, which might be attributed to the formation of the $InCrO_4$-TiO_2 sample should posses high photocatalytic activity and high antibacterial activity.

3.5. PL analysis

Photoluminescence spectra of TiO_2 and $InCrO_4$-TiO_2 are shown in respectively. As the photoluminescence occurs due to electron−hole recombination, its intensity is directly proportional to the rate of electron−hole recombination.[39] TiO_2 gave four emissions at 437, 486, 531 and 595 nm and $InCrO_4$-TiO_2 gave four emissions at 437, 486, 539 and 642 nm. $InCrO_4$-TiO_2 slightly shifts in emission compared to the undoped TiO_2 material were observed. The intensity of $InCrO_4$-TiO_2 emission is less when compared to that of TiO_2 nanomaterials.

This is because of suppression off recombination of electron−hole pairs by $InCrO_4$-TiO_2. Fig. 7a and 7b indicating that the activity difference is not due to the variation of the separation efficiency of the photogenerated electron and hole pairs. As we know, the recombination of electron and hole pairs can release energy in the form of PL emission. A low electron and hole recombination rate implies a lower luminescence emission intensity and higher photocatalytic activity.[40–42]
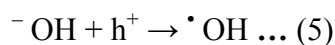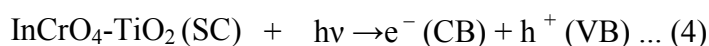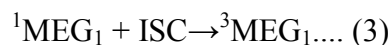
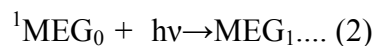### 3.6. Degradation of kinetic study

A solution of (1×10^{-4}) MEG was prepared in doubly distilled water and 0.150 g of $InCrO_4$-TiO_2 was loaded to it. The pH of the reaction mixture was adjusted to 7 and then this solution was exposed to a 200 W tungsten lamp at 60.0 m W cm^{-2}. It was observed that there was a decrease in absorbance of methyl green solution with increasing time of exposure of UV light. A linear plot between $1 + \log A$ vs time was obtained, which indicates that the photocatalytic degradation of methyl green follows pseudo-first order kinetics. The rate constant for this reaction was measured with the help of following equation[43, 44]
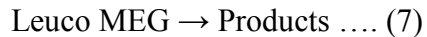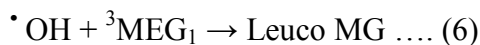
$$k = 2.303 \times slope \dots (1)$$

Discussion has been presented in Table. 1a,

3.7. Mechanism

On the basis of these observations, a tentative mechanism for photocatalytic degradation methyle green dye is proposed as follows:

$$^1MEG_0 + h\nu \rightarrow MEG_1 \dots (2)$$

$$^1MEG_1 + ISC \rightarrow {^3MEG_1} \dots (3)$$

$$InCrO_4\text{-}TiO_2\,(SC) + h\nu \rightarrow e^-\,(CB) + h^+\,(VB) \dots (4)$$

$$^-OH + h^+ \rightarrow {^\bullet OH} \dots (5)$$

$$^{\bullet}OH + {}^{3}MEG_{1} \rightarrow \text{Leuco MG} \ \dots. \ (6)$$

$$\text{Leuco MEG} \rightarrow \text{Products} \ \dots. \ (7)$$

Methyl green absorbs radiations of desired wavelength and it is excited giving its first excited. Singletstate. Further, it undergoes intersystem crossing (ISC) to give its more stable triplet state. Along with this, the semiconducting Indiumchromate-TiO_2 (SC) also utilizes this energy to excite its electron from valence band to the conduction band. An electron can be abstracted from hydroxyl ion by hole (h^+) present in the valence band of semiconductor generating $^{\bullet}OH$ radical. This hydroxyl radical will oxidize methyl green to its leuco form, which may ultimately degrade to products. It was confirmed that the $^{\bullet}OH$ radical participates as an active oxidizing species in the degradation of methyl green as the rate of degradation was appreciably reduced in presence of hydroxyl radical scavenger (2-propanol)[43] Shows in Scheme.2.

3.8. Photodegradation and decolorization of MEG

3.8.1. Primary analysis: Photodegradation and decolorization of MEG with artificial
UV- light

The photo irradiation of MEG in aqueous medium in the presence of catalyst and the atmospheric air were studied using multi lamp photoreactor with mercury UV lamps of wavelength 365 nm. The reference wavelength of MEG reaction solution is 630 nm. The intial dye concentration 1×10^{-4} M and the pH of dye is neutral (pH=7). It was shown to the dark green in colour. After the photodegradation and decolorization, the colour also, ICT is most efficient. Colour changes at irradiation times shown in respectively. The reaction time affords the photodegratation and decolorization of MEG. Thus $InCrO_4$-TiO_2 exhibited very higher

photocatalytic activity when compared to that of undoped TiO_2 and TiO_2-P25, Dark, Nil catalyst shown in Fig. 8a. The MEG dye is resistant to photolysis and for the same experiment with TiO_2 in the dye (1×10^{-4}) concentration was observed. This is because of the adsorption of dye on the catalyst. MEG undergoes % of degradation and decolorization 0, 40, 63, 72 and 88 % and 0, 43, 65, 74.5 and 92% in the presence of TiO_2 under UV-light in 60 min irradiation shown in Figure. 8b. Dye is resistant to photolysis, and for the same experiment with $InCrO_4-TiO_2$ in the dark in dye (1×10^{-4}) concentration was observed MEG undergoes % degradation and decolorization of 0, 45.7, 67.7, 84.2 and 92.8% and 0, 47, 70, 87.2 and 98.5% in the presence of $InCrO_4-TiO_2$ under UV-light in 60 min irradiation shown in Figure. 8c. The reaction time was affords the photodegratation and decolorization of MEG on $InCrO_4-TiO_2$ exhibited very higher photocatalytic activity and antibacterial activity when compared to that of TiO_2 nanomaterial.

3.8.2. Effect of pH and photocatalytic efficiency of InCrO4-TiO$_2$ on the degradation of UV-light

The pH of the solution may also affect the degradation of methyl green, malachite green and methylene blue. The effect of pH on the rate of degradation compared to fast dye methyl green was investigated in the pH range 3-11 the results are reported in Table 1b. It is observed that the degradation rate increases with an increase in pH up to 7 and then decreases. After 60 min of irradiation, the percentages of MEG degradation are 51, 70, 92, 80, 76, and 60 at pH 3, 5, 7, 9, and 11, respectively. The optimum pH is found to be 7 for MEG degradation. Low removal efficiency at the acidic pH range may be due to the dissolution of TiO_2 in $InCrO_4-TiO_2$. $InCrO_4-TiO_2$ is more effective than TiO_2 in the degradation of MEG, because it has maximum efficiency at neutral pH=7, to find out the reason for the effect of pH on degradation efficiency. Different colored dyes and (MEG-pH=7), (MG-pH=7) and (MB-pH=7) solution using the

prepared photocatalysts under UV- light irradiation in the presence of $InCrO_4$-TiO_2 high photocatalytic activity and UV- light to compared other dyes was shown in Fig.9a. The time required to obtain a clear colourless solution (92.8 % of degradation of MEG) by $InCrO_4$-TiO_2 was found to be 60 mins. The ICT on dye observed that the rate of photocatalytic degradation of methyl green increases as pH was increased and it attained optimum value at pH 7. On further increasing pH, the rate of the reaction was decreased. This behavior may be explained on the basis that as pH was increased, there is greater probability for the formation of hydroxyl radicals, which are produced from the reaction between OH ions and hole (h+) in valence band of the semiconductor, with the formation of more •OH radicals, the rate of photocatalytic degradation of the dye increases. Above pH 7, a decrease in the rate of photocatalytic degradation of the MEG was observed, which may be due to the fact that cationic form of methyl green is converted to its neutral form, which faces no attraction towards the negatively charged semiconductor surface due to adsorption of ⁻OH ions.

3.8.3. Effect of heat--treatment temperatures

The effect of calcinations on the photocatalytic activity of mixed oxides was also investigated. Shown in Fig.9b the profiles of the phodegradation of MEG under UV light irradiation using $InCrO_4$-TiO_2 mixed oxide calcined at 200 °C, 300 °C and 450°C The samples calcined at 200°C showed the highest photocatalytic activity than that calcined at other temperatures. It seems that the increase of the calcination temperature decreased the number of defect‑states on the surface. Above 200 °C temperature, the activity of catalyst decreased. It was also observed that adsorption of the MEG dye decreased with an increase of the calcination temperature of the catalyst. It seems that the increase of the calcination temperature decreased

the number of defect‑states,[45] The heat treatment of the sample at a temperature higher than 300

°C had poor photocatalytic

3.8.4. Effect of different concentrations of MEG

The effect of dye concentration was observed by taking different concentrations of methyl green. The results are summarized in Table 2a.It is important from an application point of view to study the dependence of degradation and adsorption on the concentration of dyes. Fig. 9c shows that the increase of dye concentration from 1 to 2×10^{-4} M decreases the rate constant from 0.034 to 0.02139 min^{-1}. The rate of degradation relates to $^{\bullet}OH$ (hydroxyl radical) formation on catalyst surface and probability of $^{\bullet}OH$ reacting with dye molecule. As the initial concentration of the dye increases, the path length of the photons entering the solution decreases. Thus, the photocatalytic degradation efficiency decreases,[46, 47] while at low concentration the reverse effect is observed, increasing photon absorption by the catalyst. The large amount of adsorbed dye may also have a competing effect on the adsorption of oxygen and OH^{-} onto the surface of catalyst. Different concentrations of MEG were prepared and it is used for the photodegradation and decolorization process by using UV light. Photodegradation and decolorization of MEG was high in lower concentration when compared to of it higher concentration

3.8.5. Effect of catalyst loadings

The amount of catalyst loading may also affect the degradation of dye and hence, different amounts of ICT were used. The results are reported in Table 2b.The Catalyst loading in photocatalytic processes is an important factor that can strongly influence dye degradation. Experiments performed with different amounts of $InCrO_4$-TiO_2 showed that the photodegradation efficiency increased with an increase in amount up 40 mL and then slightly

decrease as observed in. The pseudo-first-order rate constants are 0.034 and 0.0593 min^{-1} for

InCrO$_4$-TiO$_2$ at catalyst loadings of range of 0.150 g, 0.200 g and 0.250 g the total volume of

solution to uses 40 mL respectively shown in Fig 9d. This observation can be explained in terms

of availability of active sites on the catalyst surface and penetration of UV-light into the

suspension. The total active surface area increases with increasing catalyst dosage.[48] However,

with excess dosage there is a decrease in UV-light penetration as a result of an increased light

scattering effect by catalyst particles.[49] As a result, the photoactivated volume of suspension

decreases. Additionally, it is important to keep the treatment expenses low for industrial use.

Thus, we use 0.150 g as the optimal catalyst amount in our work.

3.8.6. Data Analysis

Since we tested the efficiency of this catalyst with MEG dye degradation. As shown in

(see Supporting Information), this catalyst was found to be most efficient in the degradation of

these dye also. The degradation was highly effective with InCrO$_4$-TiO$_2$, the influence of

operational parameters had been carried out to find out the optimum conditions. The

photocatalytic degradation of MEG dye containing InCrO$_4$-TiO$_2$ obeys pseudo-first-order

kinetics. At low initial dye concentration, the rate expression is given by

$$d[C]/dt = k'[C] \quad \text{------------------------ (8)}$$

where k′ is the pseudo-first-order rate constant. The dye is adsorbed onto the InCrO$_4$-TiO$_2$

surface, and the adsorption−desorption equilibrium is reached in 60 min. After adsorption the

equilibrium concentration of the dye solution is determined and taken as the initial dye

concentration for kinetic analysis. Integration of eq 8 (with the limit of C = C$_0$ at t = 0 with C$_0$

being the equilibrium concentration of the bulk solution) gives eq. 9

$$\ln (C_0/C) = k. \, t \quad \text{-------------------------------(9)}$$

where C_0 is the equilibrium concentration of dye and C is the concentration at time t. Photonic efficiency under optimum conditions for MEG dye degradation by $InCrO_4$-TiO_2 was calculated using the reported method.[50] The quantum yield of a photocatalytic reaction is defined as the number of MEG dye molecules being decomposed (degraded) per photon absorbed (eq 10).

$$\Phi = \text{Number of molecules decompose/ Number of photons of light absorbed} \text{ --------- (10)}$$

The photodegradation rate constants (k') of MEG dye under the monochromatic light source can also be used for calculation of its reaction quantum yield[50-52] using eq. 11

$$\Phi = \frac{k}{2.303 \, I_{0,\lambda} \, \varepsilon_{D\lambda} \, l} \text{ ------------ (11)}$$

where Φ is the reaction of quantum yield (dimensionless), Io is the light intensity of the incident light range at 200−800 nm range (1.381×10^{-6}), $\varepsilon_{D\lambda}$ is the molar absorptivity of MEG at 630 nm (1.0×10^{5} cm^{-1} M^{-1}), and l is the path length (1 cm) of the reaction and is for 50 mL of irradiated solution. The results of degradation quantum yields by, undoped TiO_2 and $InCrO_4$-TiO_2 are 1.1 x 10^{-2} and 6.5 x 10^{-2} mole/Einstein[32]), respectively. These results indicate that the quantum yield of the $InCrO_4$-TiO_2 process is high when compared to other processes (Table.3).

3.8.7. Stability and Reusability

The reusestability of the $InCrO_4$-TiO_2 (ICT) photocatalyst was investigated by repeating MEG degradation experiments five times. After each cycle, the $InCrO_4$-TiO_2 photocatalysts were washed thoroughly with water, and a fresh solution of MEG was made before each photocatalytic run in the photoreactor. Under UV- light and the results are shown in Fig. 10. Complete degradation occurred in the 1st, 2nd 3rd 4th at and 5th cycle obtained 100, 99, 98, 96.5

and 94.4 % degradation. The results indicats prepared catalysts are stable and reusable. Also it indicates that the photocatalytic efficiency of InCrO$_4$-TiO$_2$ was decreased slowly with increase the repetition of the fifth cycles. At the fifth cycle, 5.6 %. loss of the catalyst observed. The loss of catalyst due to the water washing, which was not much observable. Thus suggests that ICT photocatalysts have excellent stability and reliability for photodegradation of pollutants. After completion of the degradation process the solution was tested for In^{3+} leaching with sodium sulfide. There is no precipitation of Indium sulfide (black color) was formed. As there is no further leaching of In^{3+}this catalyst is nontoxic for wastewater treatment. Thus suggests that InCrO$_4$-TiO$_2$ photocatalysts have excellent stability and reusability for photodegradation of pollutants

3.8.8. Hydroxyl radical analysis

The photocatalytic activity of as-prepared samples was further confirmed by the detection of $^\bullet$OH shows the changes of the fluorescence spectra of coumarin solution under UV-light irradiation as a function of irradiation time (ICT - 0, 30 and 60 min). This result suggests that the fluorescence arises[53] from the chemical reactions between coumarin solution and $^\bullet$OH formed on the illuminated InCrO$_4$–TiO$_2$. Further observation shows that the fluorescence intensity at 365 nm further confirms the existence of hydroxyl radicals. The formed hydroxyl radicals on the surface of InCrO$_4$-TiO$_2$ samples illuminated by UV light were detected by fluorescence technique. The emission spectra excited at 320 nm in coumarin solution added with InCrO$_4$-TiO$_2$ samples were measured Fig. 11 Displays that fluorescence signal at 365 nm for different time of addition with InCrO$_4$-TiO$_2$ samples. The maximum fluorescence intensity was found for InCrO$_4$-TiO$_2$ at 60 min. This suggests that the fluorescence is caused by chemical reactions of coumarin with hydroxyl radicals formed in photocatalytic reactions.[54] Hence, hydroxyl radical is the

reactive oxidation species in InCrO$_4$-TiO$_2$ samples and finally induces the degradation of MEG. Moreover at 60 mins InCrO$_4$-TiO$_2$ sample with maximal photocatalytic activity produced much more reactive hydroxyl radicals than other samples,[55] which is also consistent with the results of photocatalytic decomposition. The hydroxyl radical analysis further confirms that the hydroxyl radicals are active species using photocatalytic reactions. On the other hand, the formation rate of $^\bullet$OH is directly related to the photocatalytic activity of InCrO$_4$-TiO$_2$ nanomaterial.

3.9. Determination of antibacterial activity by disk-diffusion method

3.9.1 Antibacterial activity of InCrO$_4$-TiO$_2$ nanomaterial

Two pathogenic bacteria using well diffusion method. The antibacterial results showed the relatively high activity against the tested pathogens exhibited comparatively low antibacterial activity. Root showed moderate activity against the tested pathogens, *Vibrato cholera* and *Bacillus subtilis* were the most resistant strains,[56-58] and medicinal plants have been main source for drugs over many centuries in many countries, in both developed and developing world. Traditional medicines products are not officially recognized in many countries, and the European Union currently developing regulatory laws for superior traditional medicines.[20] The medicinal property of plants is due to the occurrence of diverse complex chemical compounds as secondary metabolites, which are exclusively accumulated in different regions of the plants.[59] ware natural secondary metabolites are vital as potential antimicrobial crude medicine and source for natural compounds as new anti-infection agents.[60] The incidence of bacterial diseases is becoming frequent in south Asia mainly in India, because of expansion of antibacterial drug resistant pathogens. For resolve this trouble and to identify alternative chemotherapeutic agents, the exploration for new antibacterial compounds from newer sources is a global challenge[20] Quantification of total extracted carotenoids.[61] Total volume of pigmented methanolic extract

was used to quantify total carotenoid/ pigment content in bacteria according to the equation provided by

Total carotenoid content in bacteria = ATotal x volume (ml) x10000" / A1%cm x sample wt. (g)"

Where, ATotal= Absorbance at 474 nm, Volume= Total volume of extract (mL),

A1%=Absorption coefficient of carotenoids mixture in methanol.

However more work into the gene level of plants will confirm the cause of this elevated antibacterial activity from plants growing near mobile tower vicinity will confirm the cause of this elevated antibacterial activity. The present study however needs more substantiate molecular level evaluation of the mutant plants to confirm whether this change will benefit mankind in a positive manner by becoming an alternative to allopathic medicines in the present era of multiple resistant strains of micro organisms. However more work into the gene level of will confirm the cause of this elevated antibacterial activity from plants growing near mobile tower vicinity will confirm the cause of this elevated antibacterial activity. The present study however needs more substantiate molecular level evaluation of the mutant plants to confirm whether this change will benefit mankind in a positive manner by becoming an alternative to allopathic medicines in the present era of multiple resistant strains of micro organisms.[62] The result in $InCrO_4-TiO_2$ is more effective than TiO_2 in the degradation of the MEG dye. Material (1) TiO_2 and (2) $InCrO_4-TiO_2$ against the tested bacterial strains. From the zone of inhibition of the materials are tested for antibacterial activity. The TiO_2 (1) material was very poor activity against (a) *Bacillus subtilis* (positive) and (b) *Vibrio cholera* (Negative) and $InCrO_4-TiO_2$ (2) materials very batter than activity of (a) the *Bacillus subtilis* (positive) and (b)*Vibrio cholera* (Negative), when compared to that of TiO_2 shows Fig. 12. TiO_2 material is moderate and poor activity against all the tested bacterial strains. $InCrO_4-TiO_2$ has batter than antibacterial activity and high photocatalitic

activity of the nanomaterial on the nature and position of Indium and Chromate groups present in the TiO_2 material shows in Table. 4.

4. Conclusions

The heterostructrued $InCrO_4$-loaded TiO_2-coupled semiconductor photocatalyst was synthesized by co-precipitation technique and characterized by XRD, SEM with EDX, FT-IR, FT-RAMAN and PL analysis the suitable analytical method. These results confirmed the formation of $InCrO_4$-TiO_2 material XRD and SEM with showed the average particle size as 78.9 nm and 80 nm, EDX analysis showed In, Cr, Ti and O were present material identify. It showed increased absorption in the UV region. SEM analysis showed $InCrO_4$-TiO_2 has a nano-spherical like structure with high porosity. The photocatalytic activity of the catalyst was evaluated by degradation of MEG, MAG and MB in aqueous solution under UV-light. $InCrO_4$-TiO_2 was more efficient in the dye degradation than the TiO_2 and TiO_2−P25. The optimum pH and catalyst concentration for efficient removal of dye were found to be 7 and respectively. The photodegradation of MEG on $InCrO_4$-TiO_2 in aqueous medium has been studied as a function of heat-treatment temperatures, concentration of dye and amount of catalyst loading. Showed reasonable activity compared then better activity $InCrO_4$-TiO_2 nanomaterial. The mechanism of photocatalytic defnids of MEG is due to formation of hydroxyl radical analysis. The hydroxyl radical analysis further confirms that the hydroxyl radicals are active species in the photocatalytic reactions. The formation rate of OH radicals is directly related to the photocatalytic activity of $InCrO_4$-TiO_2 nanomaterial, indicated which was confirmed by the Fluorescence analysis. That the photocatalysis process in the presence of $InCrO_4$-TiO_2 offered the highest quantum yield, The material also showed better antibacterial activity *Bacillus subtilis* (Positive) and *Vibrio cholera* (Negative), bacterial strains. The prepared catalyst was found to be

reusable. Furthermore it had superior photocatalytic activity. The reported work would be more useful for industrial effluent treatment due to its dual advantage and its simplicity, more stability, reusability and antibacterial activity for expert performance.

Conflict of Interest

The authors declare no competing financial interest.

REFERENCES

[1] O. Gulnaz, A. Kaya, F. Matyar, B. Arikan, *J. Haz. Mat.,* 2004, **108**, 183-188.

[2] J. Liquiang, S. Xiaojun, S. Jing, C. Weimin, X. Zili. *Rev. Sol. energy Mater. Sol. Cells.,* 2003, **70**, 133-151.

[3] E. Forgacs, T. Csarhati, G. Oros, *Environ. Int.,* 2004, **30**, 953-971.

[4] R. Tayade, K. Pravin, R.G, Surolia,.Kulkarni, V. Raksh, *Sci. Technol. Adv. mater.,* 2007, **8**, 455-462.

[5] S. Senthilvelan, V. L. Chandraboss, B. Karthikeyan, M. Murugavelu, B. Loganathan, *AIP Conf. Proc.,* 1461, 2012, **395**; doi: 10.1063/1.4736928.

[6] V.L. Chandraboss, S. Senthilvelan, L. Natanapatham, M. Murugavelu, B. Loganathan, B. Karthikeyan, *J. Non-Cryst. Sol.,* 2013, **368**, 23–28.

[7] V.L. Chandraboss, L. Natanapatham, B. Karthikeyan, J. Kamalakkannan, S. Prabha, S. Senthilvelan, *Mater. Res. Bull.,* 2013, **48**, 3707–3712.

[8] S. Senthilvelan, V.L. Chandraboss, B. Karthikeyan, L. Natanapatham, M. Murugavelu, *Mater. Sci. Semicond. Process.,* 2013, **16**, 185–192.

[9] V. L. Chandraboss, B. Karthikeyan, J. Kamalakkannan, S. Prabha, and S. Senthilvelan, *J. Nanopart.,* Volume 2013, Pages-7, http://dx.doi.org/10.1155/2013/507161.

[10] J. D. Joshi, J. Vora, S. Sharma, C. Chirag, Patel and Ashok, B. Patel. *Asian J. of Chem.*, 2004, **2**, 1069-1075.

[11] E. Haque, J. W. Jun, S. H. Jhung, *Haz. Mate.,* 2011, **185**, 507- 11.

[12] H. K. Shon, S. Phuntsho, Vigneswaran, S. Desalin. *Water Treat.,* 2008, **225**, 235–248.

[13] T. K. Ghorai, D. Dhak, S.K. Biswas, S. Dalai, P. Pramanik *J. Mol. Catal A: Chem.,* 2007, **273**, 224-9.

[14] T. K. Ghorai, M. Chakraborty, P. Pramanik, *J. Alloys and Compds.,* 2011, **509**, 8158-64.

[15] Y. R. Do, W. Lee, K. Dwight, A. Wold. *J. Solid State. Chem.*, 1994, **108**, 198.

[16] J. Papp, S. Soled, K. Dwight, A. Wold, *Chem. Mater.,* 1994, **6**, 496-500.

[17] L. Xu, E.M.P. Steinmiller, SE. Skrabalak, *J. Phys. Chem. C.,* 2012**, 116**, 871-7.

[18] X. Fu, LA. Clark, Q. Yang, M.A. Anderson, *Environ. Sci. Technol.,* 1996, **30**, 647-53.

[19] J. Yin, Zou, J. Ye, *Chem. Phys. Lett.,* 2003**, 378**, 24-8.

[20]. Robinson MM. Classifications, Terminology and Standards, WHO, Geneva: Xiaorui Zhang Traditional Medicines, WHO. Traditional medicines: global situation, issues and challenges. Edn 3rd, 2011.

[21] T. Essawi, M. Srour, *J. Ethnopharmacol.,* 2000, **70**, 343-349.

[22] G. Mijovic, B. Andric, D. Terzic, M. Lopicic, B. Dupanovic, *Journal of IMAB-Annual Proceeding (Scientific Papers).* , 2012, **18**, 216-219.

[23] P. Sumathi, A. Parvathi, *J. Med. Plants Res.,* 2010, **4**, 316-321.

[24] K. B. Oh, J. H Lee, S.C. Chung, J. Shin, H. J. Shin, H. K. Kim, et al, *Bioorg. Med. Chem. Lett.,* 2008, **18**, 104–108.

[25] K. Vallinayagam, R. Arumugam, G. Ragupathy Raja kannan, *Global J. Pharmacol.,* 2009, **3**, 50-52.

[26] T.M. Lopez Goeme, M.A. Alvarez Lemus, V. Angeles Morales, E. Gomez Lopez, P. Castillo Ocampo, *J. Nanomed. Nanotechnol.,* 2012, 1, 7.

[27] L.M. Matuana, D.P. Kamdem, J. Zhang, *J. Appl. Polym. Sci.,* 2001, **80**, 1943–1950.

[28] D.L. Pavia, G.M. Lampman, G.S. Kriz, J.A. Vyvyan, *Introduction to Spectroscopy*, 4th ed., Brooks/Cole, Belmont, CA, 2009.

[29] K.M. Joshi, V.S. Shrivastava, *Int. J. Nano Dim.,* 2012, **2,** 241-252.

 [30] W. Jiang, J.A. Joens, Dionysios D. Dionysiou, K. E. O'Shea, *J. Photochem and Photobiol. A: Chem*., 2013, **262,** 7– 13.

 [31] W. Jiang 2013, **11,** 13 *Florida International University*, <u>wjian001@fiu.edu</u>.

[32] Gusfiyesi, Admin Alif, Hermansyah Aziz, Syukri Arief and Edison Munaf. *Res. J. Pharm. Biol. Chem. Sci.,* 2014, **5,** 918.

[33] B.N. Khare, M. Meyyappan, A.M. Cassell, C.V. Nguyen, *J. Nano Letters.,* 2002, **2,** 73–77.

[34] J. Wang, T. Ma, Z. Zhang, X. Zhang, Y. Jiang, W. Sun, R. Li, P. Zhang, *Ultrason. Sonochem.,* 2007, **14,** 575–582.

[35] B. Ding, H. Kim, C. Kim, M. Khil, S. Park, *Nanotechnolol.,* 2003, **14**, 532–537.

[36] B.P. Singh, S. Nayak, S. Samal, S. Bhattacharjee, L. Besra, *Appl. Surf. Sci., 2012*, **258**, 3524–3531.

[37] U. Balachandran, N.G. Eror, *J. Solid State Chem.,* 1982, **42,** 276– 282.

[38] M. Mikami, S. Nakamura, O. Kitao, H. Arakawa, *Phys. Rev. B: Condensed* Matter*, Mater. Phys.,* 2002, **66**, 155–213.

[39] B. Subash, B. Krishnakumar, R. Velmurugan, M. Swaminathan and M. Shanthi, *Catal. Sci. Technol.,* 2012, **2**, 2319–2326.

[40] J. Zhong, F. Chen and J. L. Zhang, *J. Phys. Chem. C.,* 2010, **114**, 933–9.

[41] J. Cao, B.D Luo, H. L Lin, B. Y. Xu and S.F .Chen, *J. Hazard. Mater.,* 2012, **217**, 107–15.

[42] S.Y. Wu, H. Zheng, Y.W. Lian, and Y.Y. Wu, *Mater. Res. Bull.*, 2013, **48**, 2901−7.

[43] K. Ameta, P. Tak, D. Soni and suresh, C.ameta. *Sci. Revs. Chem. Commun.,* 2014, **4**, 38-45.

[44] K. Ameta, A. Porwal, K. L. Ameta and suresh, C. ameta, *j. Curr. Chem. Pharm. Sc.,* 2014, **4,** 65-72.

[45] K. Tanmay, Ghorai, Niladri Biswas, *J. Mater. Res. Technol.,* 2013, **2**, 10-17.

[46] B. Subash, B. Krishnakumar, V. Pandiyan, M. Swaminathan, M. Shanthi, *Sep. Purif. Technol.,* 2012, **96**, 204−213.

[47] B. Krishnakumar, K. Selvam, R. Velmurugan, M. Swaminathan, *Desalin. Water Treat.,* 2010, **24**, 132−139.

[48] B. Krishnakumar, B. Subash, M. Swaminathan, *Sep. Purif. Technol.,* 2012, **85**, 35−44.

[49] R. Velmurugan, K. Selvam, B. Krishnakumar, M. Swaminathan, *Sep. Purif. Technol.,* 2011, **80**, 119−124.

[50] B. Subash, B. Krishnakumar, M. Swaminathan, and M. Shanthi, *Langmuir.,* 2013, **29**, 939−949.

[51] N. Daneshvar, S. Aber, M. S. Seyed Dorraji, A. R. Khataee, and M. H. Rasoulifard, *Int, J. Chem. Nucl. Metall. Mater. Eng.,* 2007, **5,**

[52] W. K. Choy, W. Chu, *Chemosphere.,* 2007, **66,** 2106-2113.

[53] Q. Xiang, Jiaguo Yu and Mietek Jaroniec, *Phys. Chem. Chem. Phys.,* 2011, **13**, 4853–4861 4853.

[54] K.I. Ishibashi, A. Fujishima, T. Watanabe and K. Hashimoto, *Electrochem. Commun.,* 2000. **2**, 207−10.

[55] L. Wei Cheng, J. Chien Tsai, T. Yun Huang, C. Wei Huang, B. Unnikrishnan and Y. Wei Lin, *Mater. Res. Express.,* 2014, **1,** 025023, 2053-1591/14/025023+19$33.00.

[56] M.P. Krishna, Rinoy Varghese, A.A. Mahesh Mohan, Mohamed Hatha, *Int. J. Herbal Medi.,* 2014, **2**, 132-134.

[57] M. Alwarsamy and R. Ravichandran, *Int. J. Innovative Res. Sci, Eng. Technol.,* **2014, 3,** 1**.**

[58] V.N. Ariharan, and P. Nagendra Prasad, *Rasayan J. Chem.,* **2014**, **7,** 260 – 263.

 [59] H. Koochak, S.M Seyyednejad, Motamedi, *Asian Pacific J. Tropical Med.,* 2010, **3**, 180-184.

[60] S. C. Dwivedi, R. Dudey, R. Tyagi, M. Masand, U. Advani, *Int. J. Pharm. Res. Dev.,* 2011, **3**, 24-30.

[61] D. B. Rodriguez-Amaya, & M. Kimura, 2004, HarvestPlus Handbook for Carotenoid Analysis. HarvestPlus Technical Monograph 191 Series2; IFPRI: Washington, DC, USA, and CIAT: Cali, Colombia.

[62] S. U. Devi and B. Lawrence, *Biosci. Discovery.,* 2014, **5**, 221-226.

CAPTIONS FOR SCHEME AND FIGURES

Fig. 1. Chemical structure of (a) Methyl green

Fig. 2. XRD patterns of (a) undoped TiO_2 and (b) $InCrO_4$-TiO_2 nanomaterial.

Fig. 3. (a) SEM image (b) EDX elemental analysis, (c) image profile and selected area highlighted (d) plot profile and selected area highlighted in fig. 3(a) of the TiO_2 nanomaterial.

Fig.4. $InCrO_4$-TiO_2 nanomaterial (a,b) SEM images (c) EDX elemental analysis (d) image profile and (e) plot profile of the selected area in fig.4 (b) of the $InCrO_4$-TiO_2 nanomaterial

Fig. 5. FT-IR spectrum of a) TiO_2, b) $InCrO_4$- TiO_2 nanomaterial before photodegradation of MEG and c) $InVO_4$- TiO_2 nanomaterial after photodegradation of MEG.

Fig. 6. FT-Raman spectrum of $InCrO_4$-TiO_2 nanomaterial

Fig. 7. PL spectrum of (a) undoped TiO_2 and (b) $InCrO_4$-TiO_2 nanomaterial.

Fig. 8.(a) Primary analysis UV-light: Dark, Nil catalyst, TiO_2-P25, and % of Photodecolorization and degradation of MEG by (b) TiO_2 and (c) $InCrO_4$-TiO_2 nanomaterial.

Fig. 9. Fig.9. Effect of photocatalytic efficiency (a) Effect of ICT on different dyes and pH=7(MEG-pH=7, MG-pH=7, MB-pH=7), (b). The effect of calcination temperature (200, 300 and 450^0C) of MEG dye, (c) different concentration of MEG dye and (d) Different catalyst loading of MEG dye UV-light study of their photocatalytic activity.

Fig. 10. Catalyst reusability, $InCrO_4$-TiO_2 on MEG ($1x10^{-4}$) dye under UV-light irradiation time 60 min.

Fig. 11. Fluorescence spectra measured at λmax = 320 nm for the $InCrO_4$-TiO_2 samples obtained using various time (0, 30 and 60 min) in coumarin solution (sample was illuminated for 60 min of UV light).

Fig.12. Antibacterial activity of [disc diffusion method] (a) *Bacillus subtilis* (positive) (b) *Vibrio cholera* (Negative)

**Scheme. 1**. Preparation of $InCrO_4 - TiO_2$ nanomaterial.

Scheme. 2. Schematic representation for the photogeneration of holes and electrons in the $InCrO_4-TiO_2$ nanomaterial upon UV light for successive mineralization of MEG.

Table. 1. (a) A Typical run time, absorbence in precence of rate constant value and (b) Effect of pH

Table. 2 (a) Effect of methyl green concentration and (b) Effect of Catalyst loading in presence of rate constant value.

Table. 3 Kinetics data of photocatalytic degradation of MEG in aqueous solution after 1 hour UV irradiation on to TiO_2 and $InCrO_4-TiO_2$.

Table.4. Antibacterial activity [disc diffusion method] (a) *Bacillus subtilis* (positive) and (b) *Vibrio cholera* (Negative) bacterial strains.
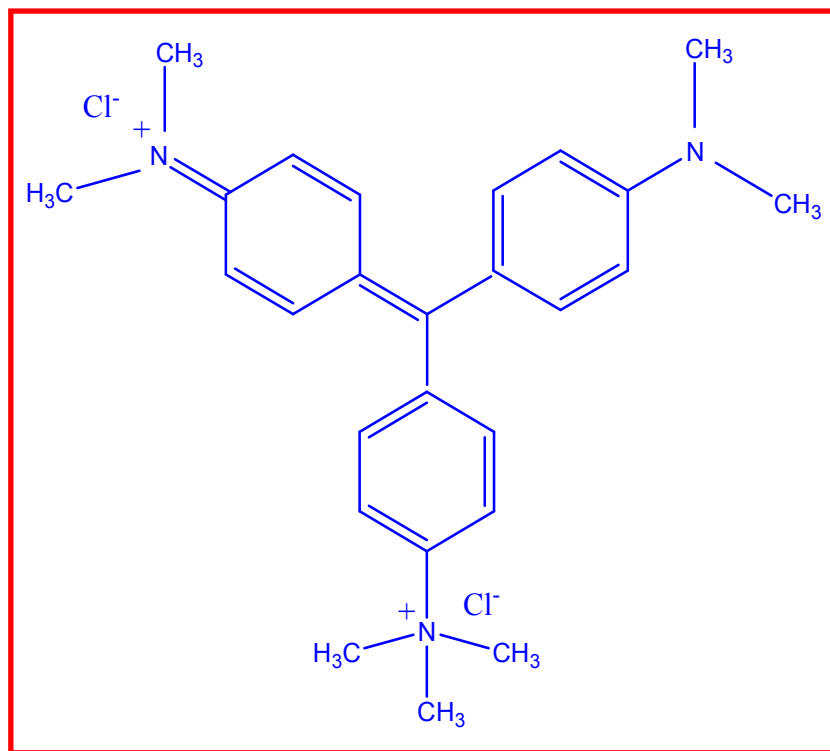
Fig. 1. Chemical structure of methyl green
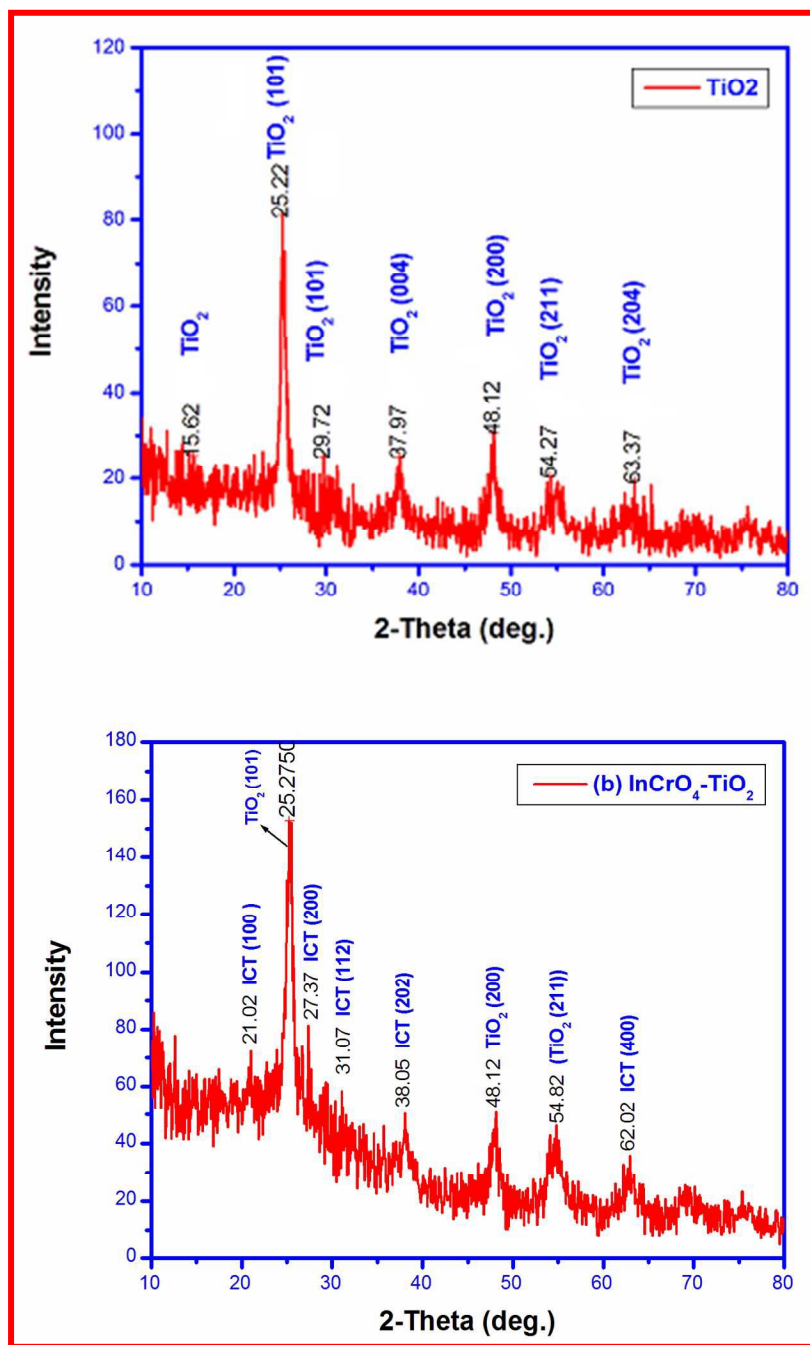
Fig. 2. XRD patterns of (a) undoped TiO_2 and (b) $InCrO_4$-TiO_2 (ICT) nanomaterial.
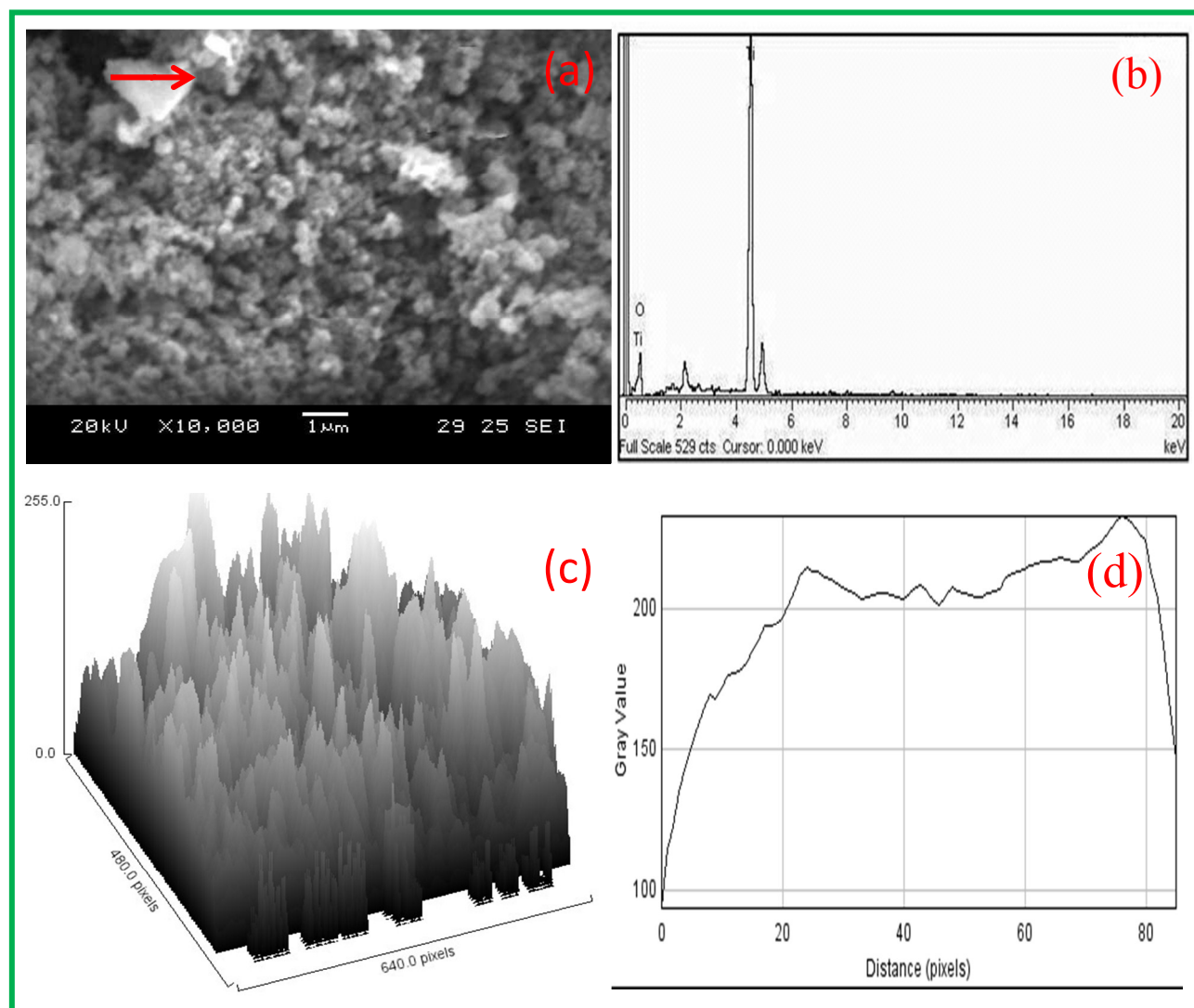
Fig. 3. (a) SEM image (b) EDX elemental analysis, (c) image profile and selected area highlighted (d) plot profile and selected area highlighted in fig. 3(a) of the TiO$_2$ nanomaterial.
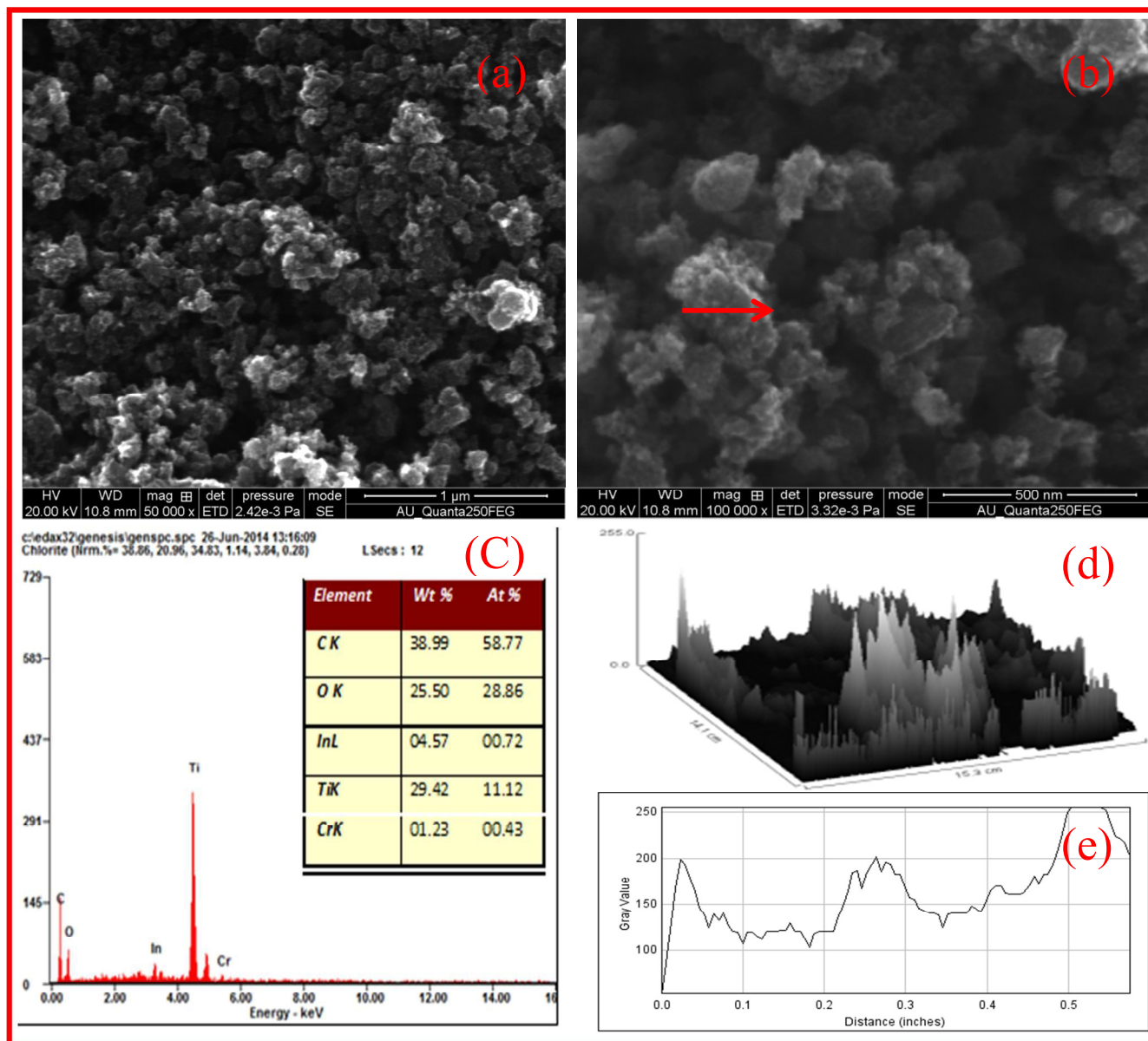
Fig.4. InCrO$_4$-TiO$_2$ nanomaterial (a,b) SEM images (c) EDX elemental analysis (d) image

profile and (e) plot profile of the selected area in fig.4 (b) of the InCrO$_4$-TiO$_2$ nanomaterial
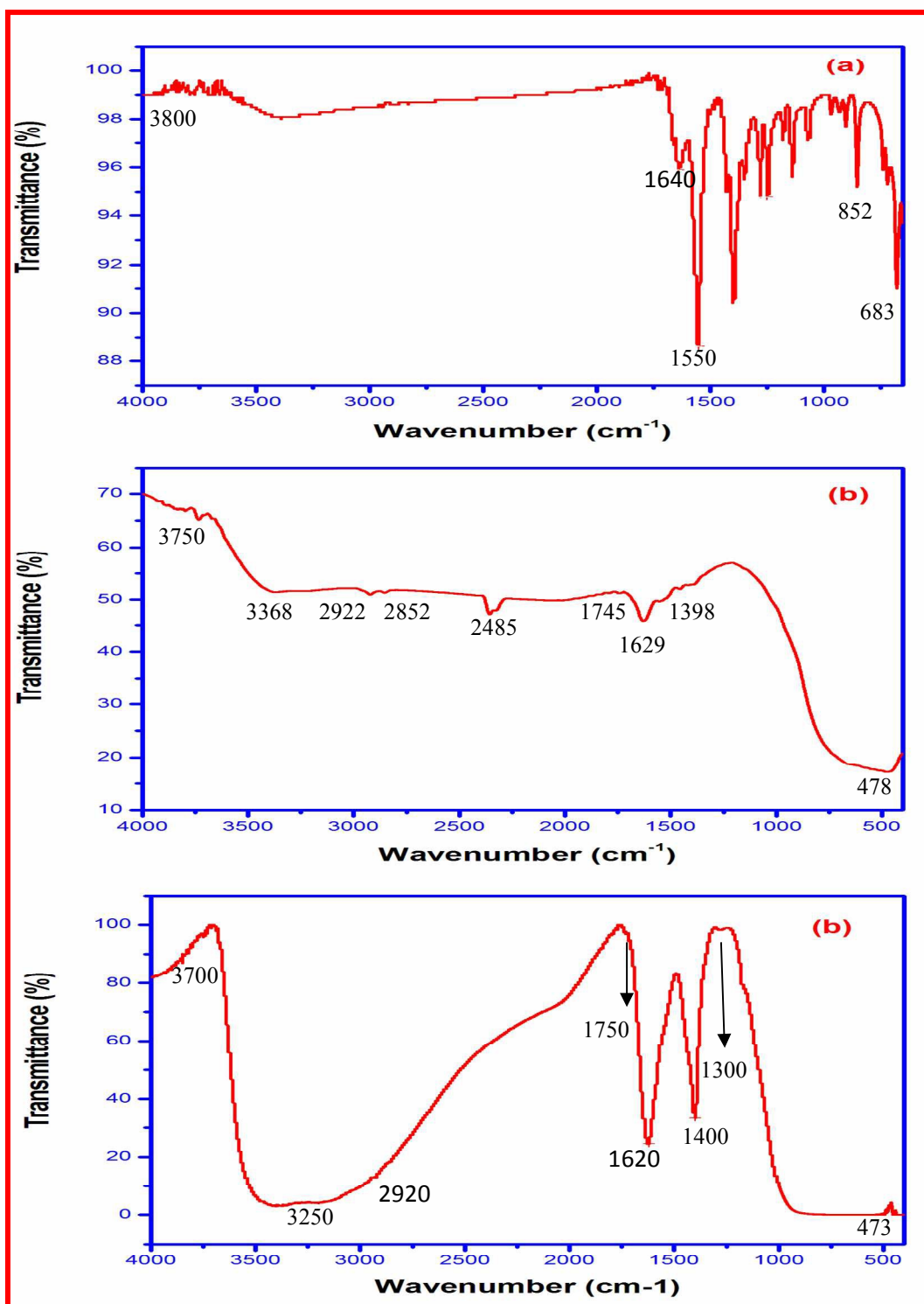
Fig.5. FT-IR spectrum of a) TiO$_2$, b) InCrO$_4$- TiO$_2$ before photodegradation of MEG and

c) InCrO$_4$- TiO$_2$ after photodegradation of MEG.
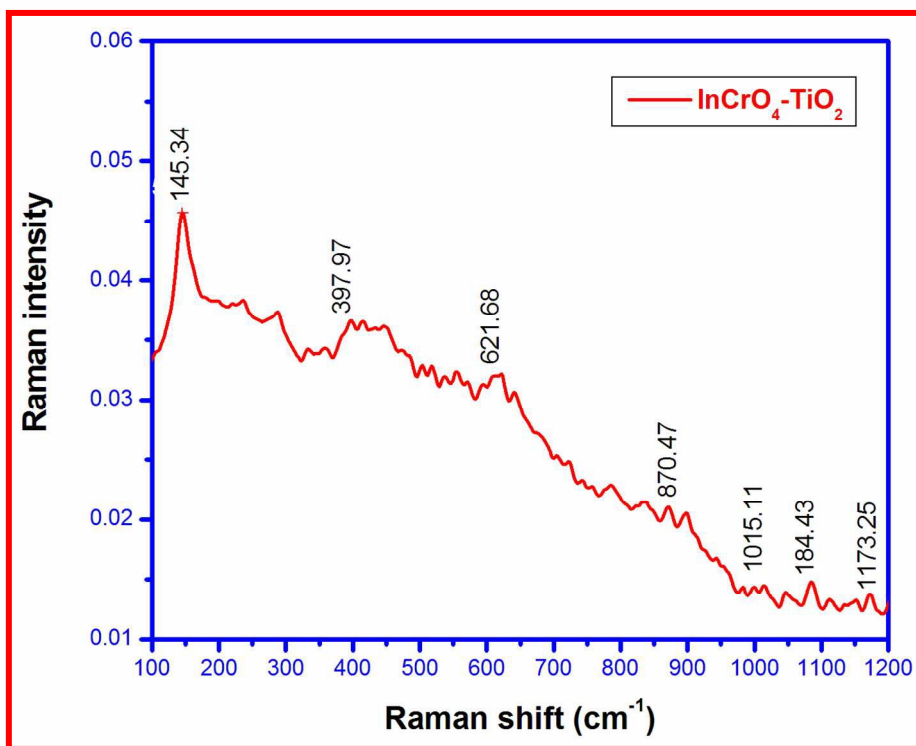
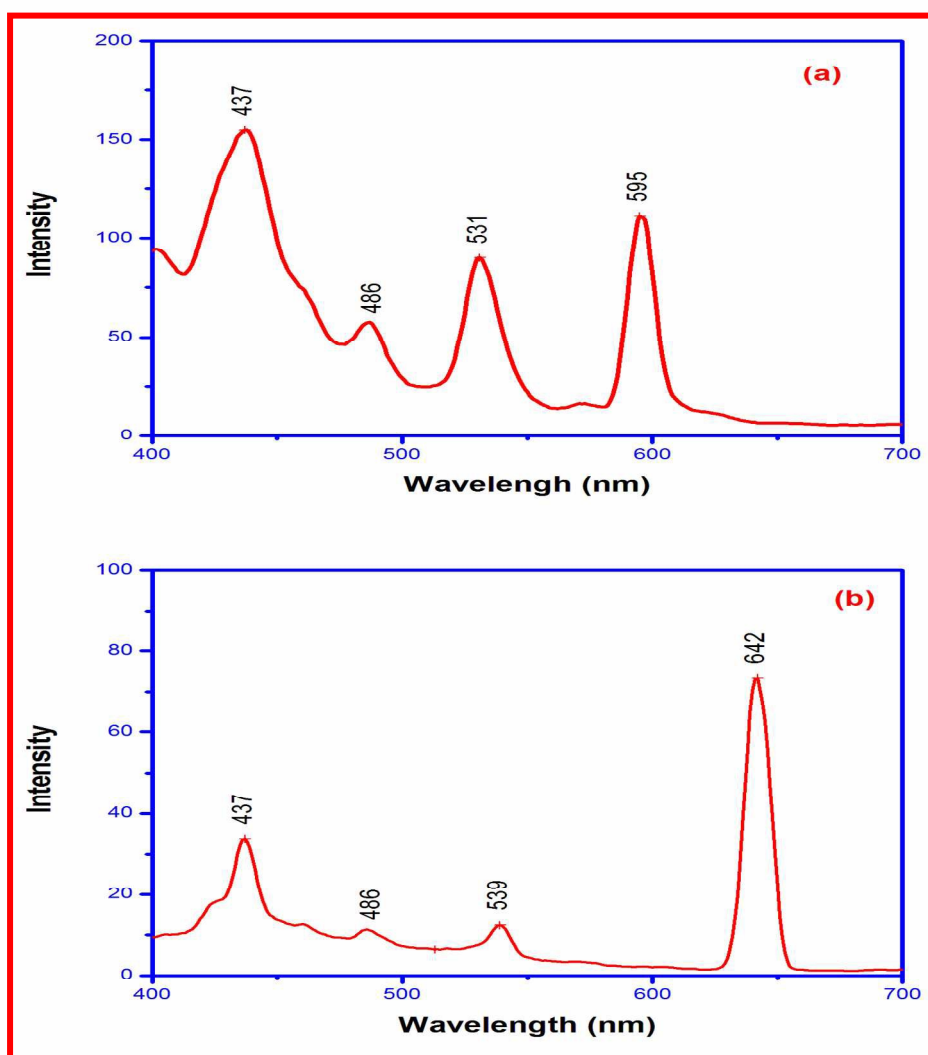**Fig.6**. FT-Raman spectrum of InCrO$_4$-TiO$_2$ nanomaterial

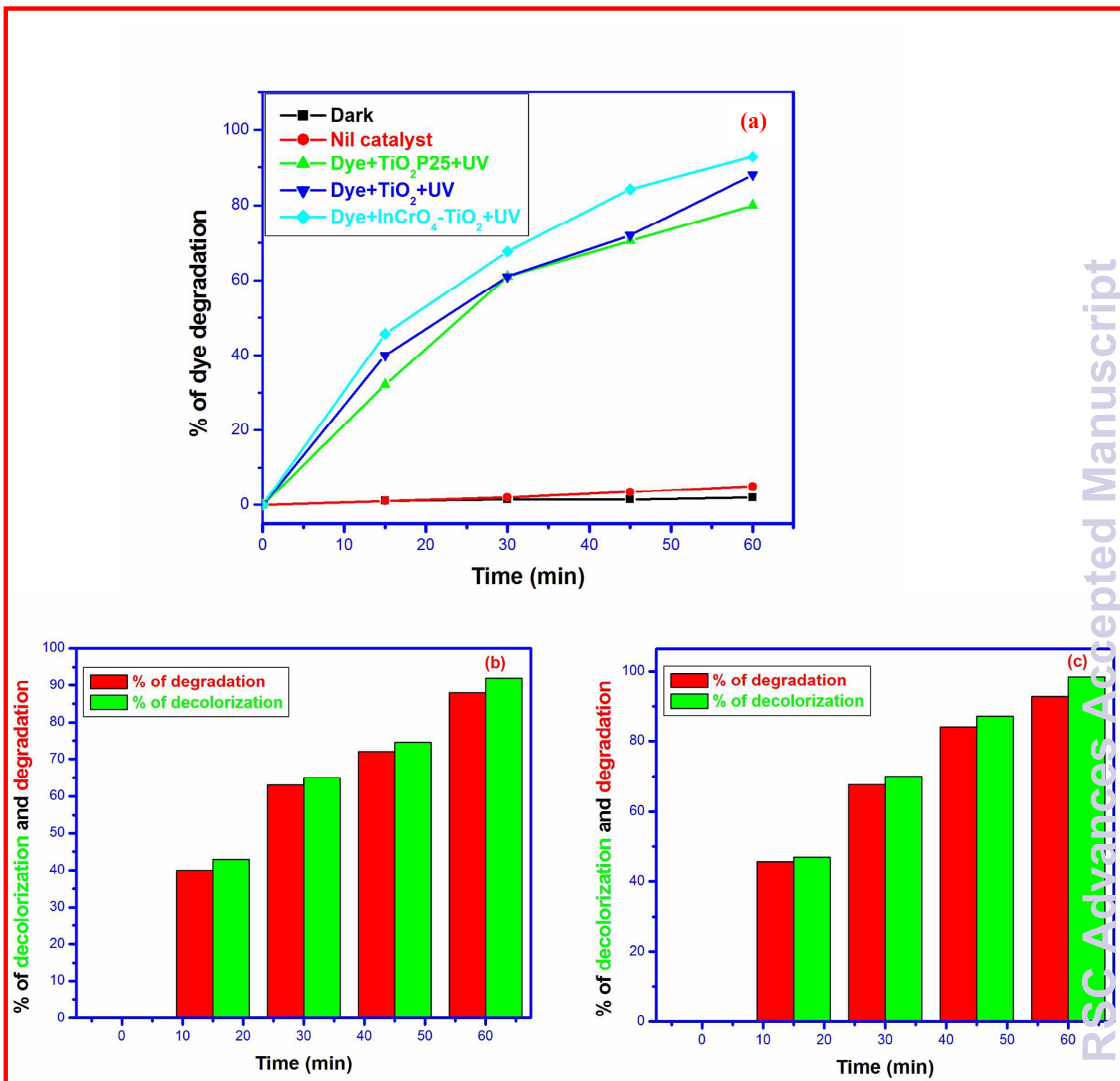**Fig. 7. PL** spectrum of (a) undoped TiO_2 and (b) $InCrO_4$-TiO_2 nanomaterial.

Fig.8. (a) Primary analysis of UV-light: Dark, Nil catalyst, TiO_2-P25 and % of photodecolorization and degradation of MEG by (b) TiO_2 and (c) $InCrO_4$-TiO_2 nanomaterial.
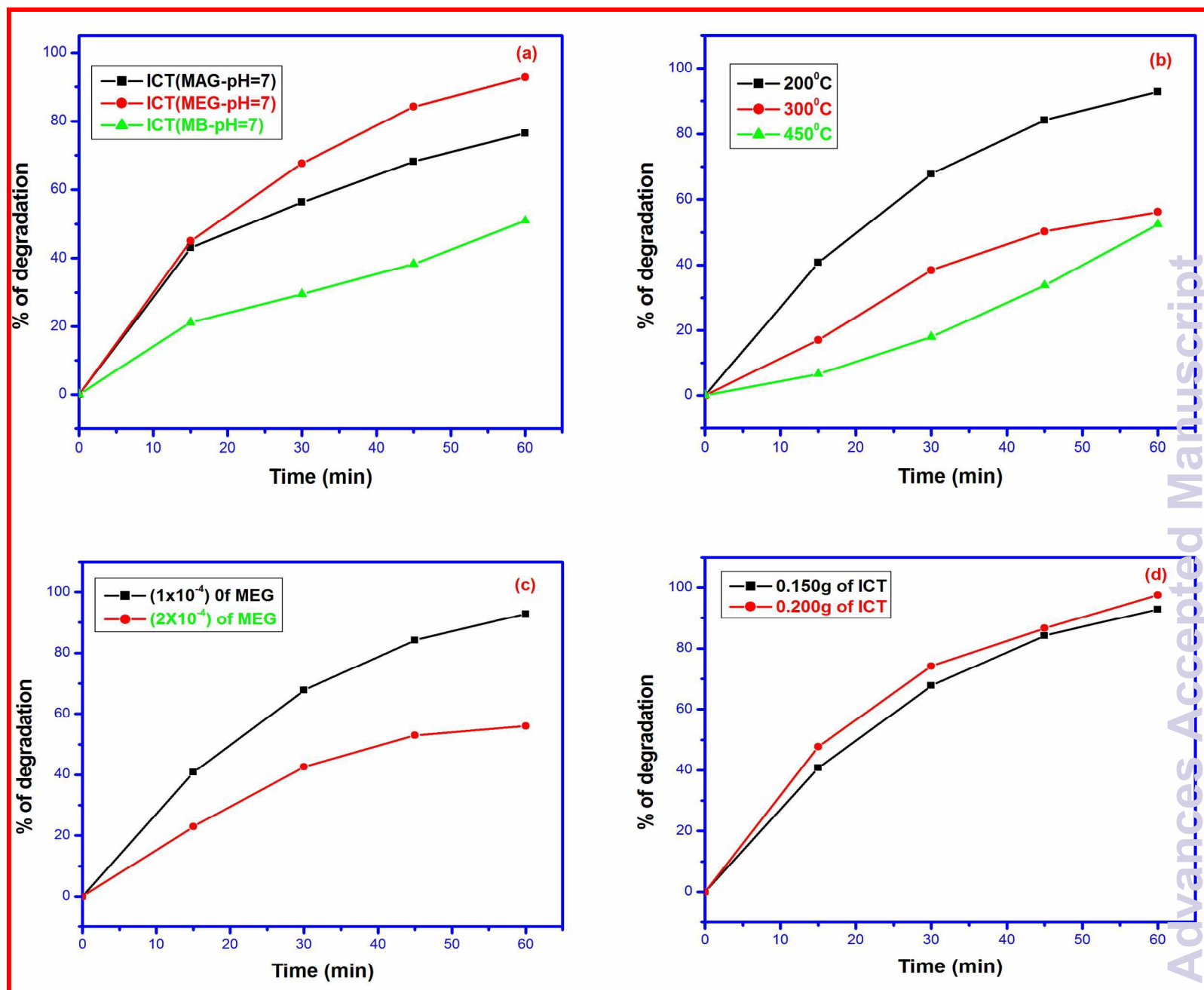
Fig.9. Effect of photocatalytic efficiency (a) Effect of (InCrO$_4$-TiO$_2$) ICT on different dyes and pH=7(MEG-pH=7, MG-pH=7, MB-pH=7), (b). The effect of calcination temperature (200, 300 and 450^{0}C) of MEG dye, (c) different concentration of MEG dye and (d) Different catalyst loading of MEG dye UV-light study of their photocatalytic activity.
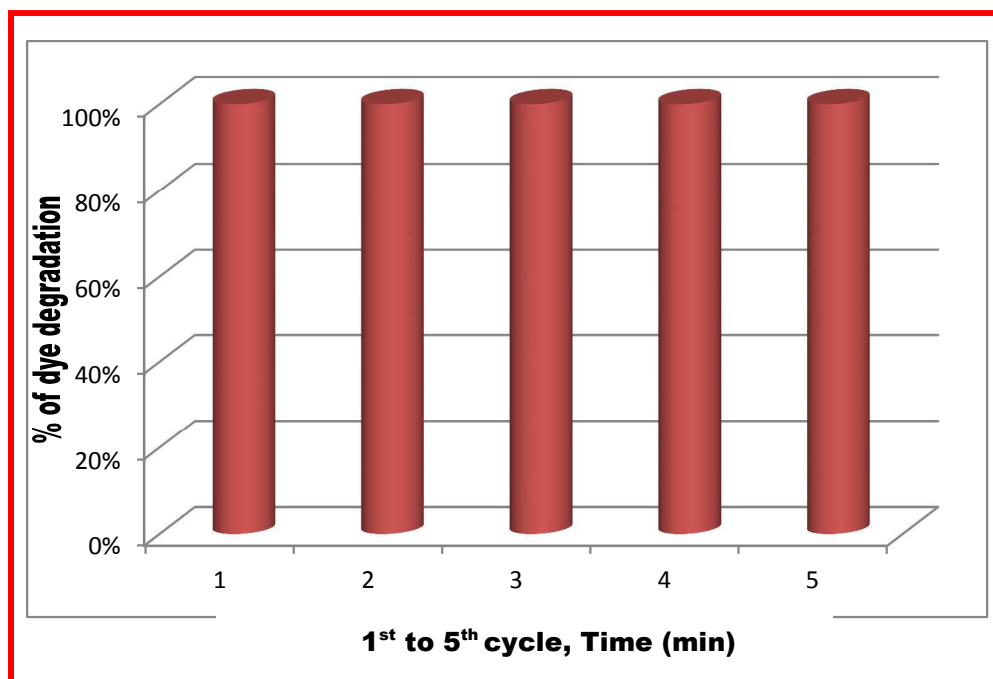
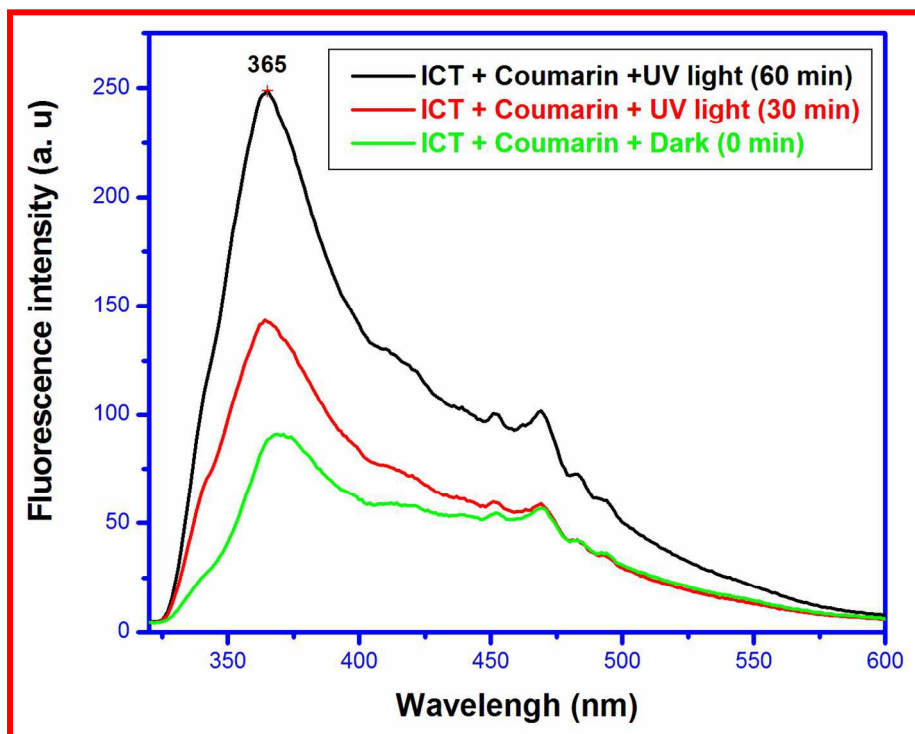**Fig. 10** Catalyst reusability, InCrO$_4$-TiO$_2$ on MEG (1x10^{-4}) dye under UV-light irradiation time 60 min.

Fig.11. Fluorescence spectra measured at λmax = 320 nm for the InCrO$_4$-TiO$_2$ samples obtained using various time (0, 30 and 60 min) in coumarin solution (sample was illuminated for 60 min of UV light).
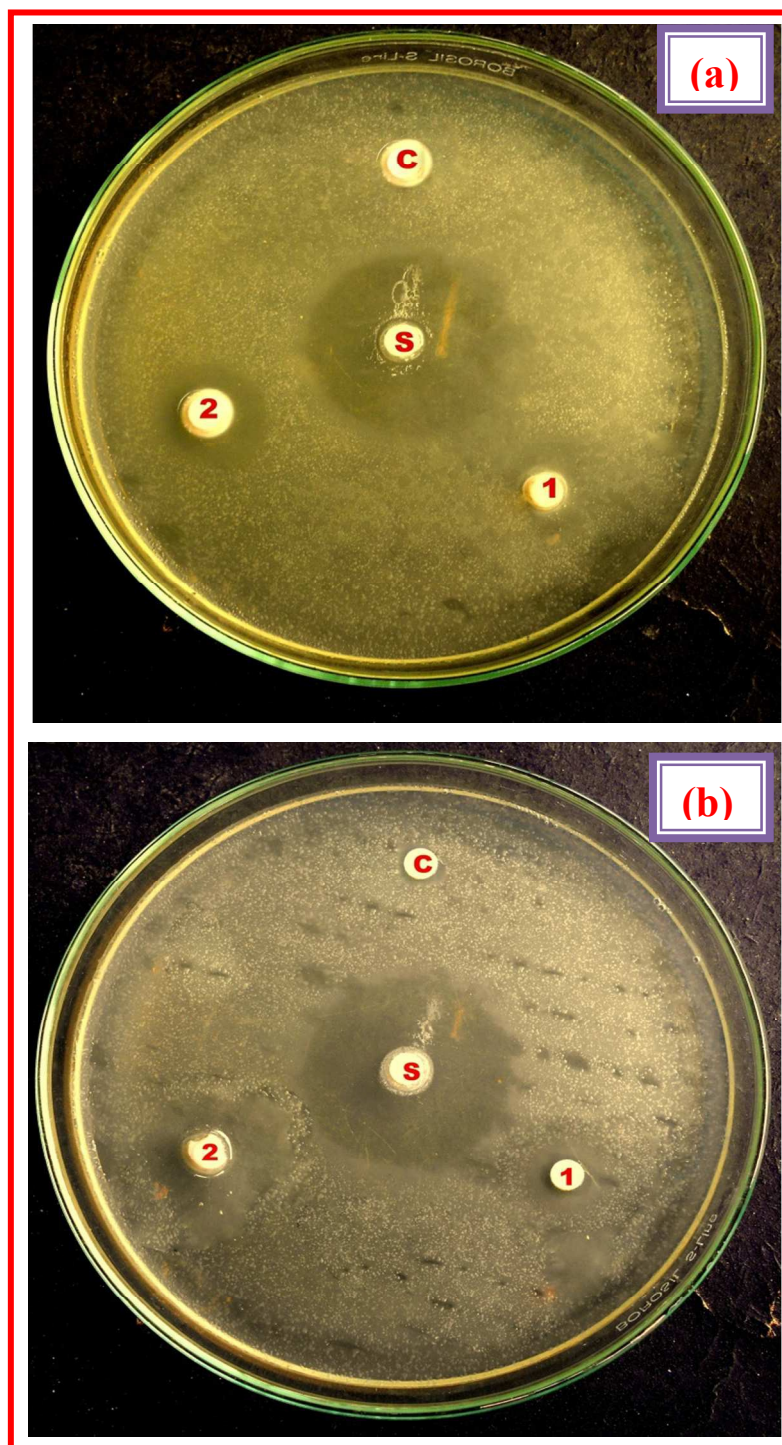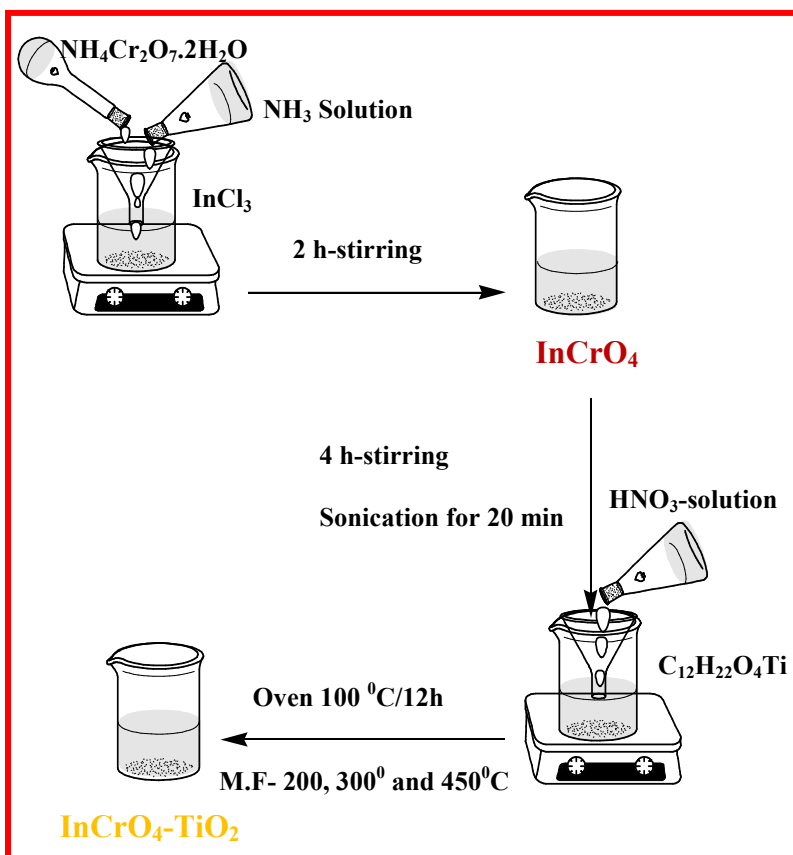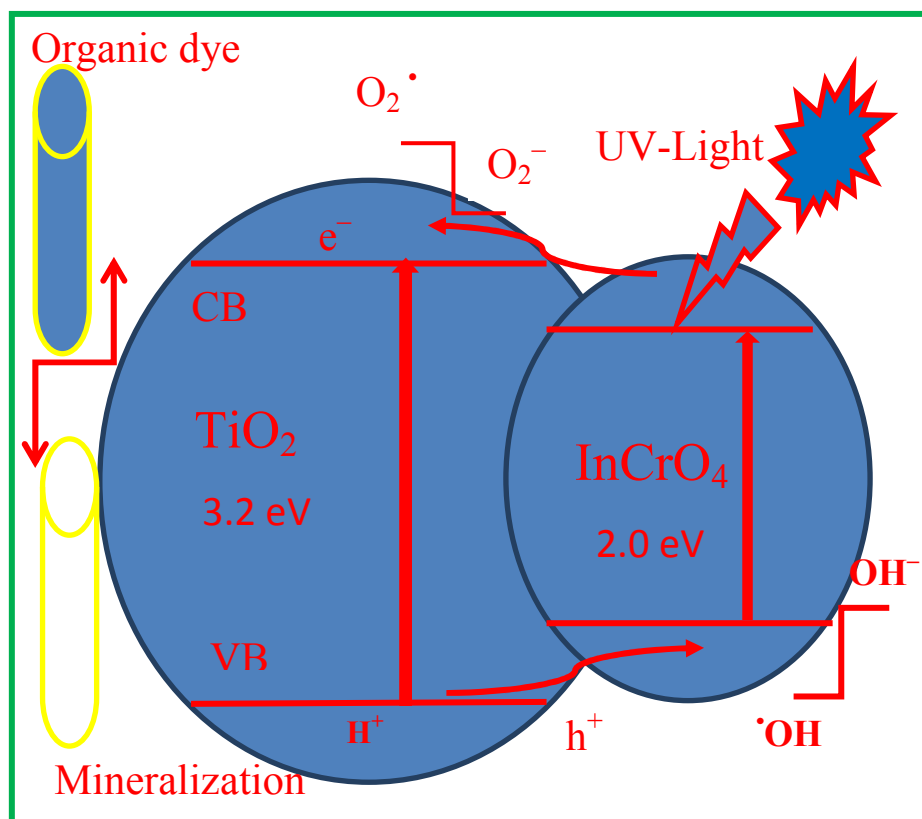
Fig.12. Antibacterial activity of [disc diffusion method] (a) *Bacillus subtilis* (positive) (b) *Vibrio cholera* (Negative)

Scheme.1. Preparation of InCrO$_4$-TiO$_2$

Scheme. 2. Schematic representation for the photodegradation holes and electrons in the InCrO₄-TiO₂ nanomaterial under UV- light for successive mineralization of MEG.

Table. 1. (a) A Typical run time, absorbence in precence of rate constant value and 1 (b) Effect of pH

(a) A Typical run

pH = 7 , [Methyl green] = 1 × 10^{-4} M   InCrO$_4$-TiO$_2$ = 0.150 g

                                                   Light Intensity= 60.0 mWcm^{-2}

Time (min.)	Absorbance (A)	1 + log A
0	0.635	0.8027
15	0.355	0.5502
30	0.205	0.3117
45	0.195	0.2900
60	0.130	0.1139

- InCrO4-TiO2 -Rate constant (k) = 2.0685 × 10^{-4} sec-1

(b) Effect of pH   InCrO$_4$-TiO$_2$ = 0.150 g

[Methyl green] 1× 10^{-4} M   Light Intensity = 60.0 mWcm^{-2}

pH	Rate constant (k) × 10^{-4} (sec-1)
3	1.13
5	1.15
7	**2.06**
9	1.68
11	1.13

Table. 2 (a) Effect of methyl green concentration and (b) Effect of Catalyst loading in presence of rate constant value.

(a) Effect of methyl green concentration

pH = 7

	Light intensity = 60.0 mWcm^{-2}
[Methyl green] × 10^{-4}	Rate constant (k) × 10^{-4} (sec^{-1})
1.00	2.068
2.00	1.2834

(b) Effect of Catalyst loading

pH = 7

Methyl green 1x10^{-4} M

Light intensity = 60.0 mWcm^{-2}

InCrO$_4$-TiO$_2$ (g)	Rate constant (k) × 10^{-4} (sec^{-1})
0.015 g	2.068
0.200 g	1.1958

Table. 3 Kinetic data of photocatalytic degradation of MEG in aqueous solution after 60 mins

Catalyst	Degradation (%)	k (menit^{-1})	$t_{1/2}$ (menit)	R^2	Quantum yield (Mole/Einsten).
TiO_2	88	0.065	12.158	0.040	1.1×10^{-2}
$InCrO_4$-TiO_2	92.8	0.034	12.501	0.014	6.5×10^{-2}

Table. 4 Antibacterial activity result by disc diffusion method

S.No.	Bacteria	Standard Antibiotic[*]	Zone of inhibition (mm)		
		Disc	1 [TiO_2]	2 [$InCrO_4$-TiO_2]	Control (DMSO)
1.	Bacillus subtilis (positive)	28	14	16	-
2.	Vibrio cholera (Negative)	30	13	16	-

*ciprofloxacin